

# Optics Letters

## High-efficiency optical parametric chirped-pulse amplifier in $\text{BiB}_3\text{O}_6$ for generation of 3 mJ, two-cycle, carrier-envelope-phase-stable pulses at $1.7 \mu\text{m}$

YANCHUN YIN,<sup>1,†</sup> JIE LI,<sup>1,†</sup> XIAOMING REN,<sup>1,†</sup> KUN ZHAO,<sup>1,2</sup> YI WU,<sup>1</sup> ERIC CUNNINGHAM,<sup>1</sup> AND ZENGHU CHANG<sup>1,\*</sup>

<sup>1</sup>Institute for the Frontier of Attosecond Science and Technology, CREOL and Department of Physics, University of Central Florida, Orlando, Florida 32816, USA

<sup>2</sup>Beijing National Laboratory for Condensed Matter Physics, Institute of Physics, Chinese Academy of Sciences, Beijing 100190, China

\*Corresponding author: Zenghu. Chang@ucf.edu

Received 15 December 2015; revised 29 January 2016; accepted 1 February 2016; posted 2 February 2016 (Doc. ID 255667); published 8 March 2016

**We produce a 3 mJ, two-cycle (11.4 fs), 1 kHz, carrier-envelope phase (CEP)-stable laser source at  $1.7 \mu\text{m}$  via a three-stage Ti:sapphire-pumped optical parametric chirped-pulse amplifier in  $\text{BiB}_3\text{O}_6$ . We achieve a pump-to-signal conversion efficiency of 18% in the last stage, which is, to the best of our knowledge, the highest yet achieved for near-octave bandwidth amplification. A f-to-2f measurement shows a CEP instability of 165 mrad over 1 h. This is an ideal light source for generating isolated attosecond pulses in the soft x-ray region.** © 2016 Optical Society of America

**OCIS codes:** (320.7090) Ultrafast lasers; (190.4970) Parametric oscillators and amplifiers.

<http://dx.doi.org/10.1364/OL.41.001142>

Attosecond science, emerging at the onset of the 21st century, has opened a new era of understanding electron dynamics and correlations which occur on attosecond timescales [1]. So far, isolated attosecond pulses as short as 67 as have been generated in an extreme ultraviolet (XUV) wavelength range by using spectrally-broadened Ti:sapphire lasers operating in the visible to near-infrared spectral region [2]. Rapid development of few-cycle, long-wavelength driving lasers has occurred in recent years to further reduce the pulse duration toward 24 as (one atomic unit of time) and cover the water-window region of the soft x-ray domain for ultrafast chemistry, condensed matter, and biologic applications [3]. Such light sources, however, are limited to low brightness because of the low pulse energy of available few-cycle IR driving lasers and the dramatically reduced single-atom response due to the quantum diffusion of electron wave packets [4–6]. Therefore, the development of high-energy few-cycle IR laser sources is in strong demand.

IR pulses with both high-pulse energies and few-cycle durations are primarily enabled by optical parametric chirped pulse amplification (OPCPA) pumped by few-picosecond (ps)

lasers, which allows a trade-off between the gain bandwidth and the damage threshold of the nonlinear crystals [7,8]. While a number of kHz-repetition rate, few-cycle, high-energy IR OPCPA sources have been reported [9–13], only two of these systems yielded mJ-level near-octave pulses (two cycles and below): the 3 kHz, 1.2 mJ,  $2.1 \mu\text{m}$  source pumped by a Yb:YAG laser in [10] and the 1 kHz, 1.5 mJ,  $1.6 \mu\text{m}$  source pumped by a Ti:sapphire laser in [13]. While commercially available Yb:YAG pump lasers with hundreds of mJ of pump energy may facilitate OPCPA output energies scaled to tens of mJ in the future, the pump-to-signal conversion efficiency of the Yb:YAG-pumped near-octave OPCPA in [10] was limited to around 7%. On the other hand, the previously reported highest efficiency in a Ti:sapphire-pumped near-octave OPCPA was 12%, achieved in a  $\text{BiB}_3\text{O}_6$  (BIBO)-based system [13]. Better understanding of the Ti:sapphire pumping scheme is interesting, since researchers can develop such an OPCPA either by making use of the existing Ti:sapphire lasers in their labs or by taking advantage of the mature high-energy Ti:sapphire products that have become available from several companies. In this Letter, we report a method for further increasing the pump-to-signal conversion efficiency of a Ti:sapphire-pumped near-octave, mJ-level OPCPA to 18% by designing the ideal Ti:sapphire pumping bandwidth and center wavelength for optimizing the complex phase matching (PM) between a linearly stretched polychromatic pump pulse and a nonlinearly stretched seed pulse. The implementation of this technique in a BIBO-based OPCPA yielded 3 mJ, two-cycle, 1 kHz, carrier-envelope phase (CEP)-stable pulses at  $1.7 \mu\text{m}$ .

In BIBO, it has been calculated previously that 780 nm light is optimal for pumping an octave-spanning spectrum centered at  $1.6 \mu\text{m}$  when using Type 1 PM [14]. Rather than tailoring the pump bandwidth and central wavelength for optimizing PM conditions, however, many BIBO-based optical parametric amplification (OPA) and OPCPA systems have been content to operate with pump wavelengths centered instead around 800 nm, which corresponds conveniently to the peak gain

of room-temperature Ti:sapphire [11,14,15]. This is reasonable for OPA systems, because the specifications for pump wavelengths are less stringent: since the near-transform-limited pump and signal pulses allow all pump wavelengths to be phase-matched with the signal wavelengths simultaneously, PM in the temporal domain is essentially uniform and straightforward. In OPCPA systems, however, the pump spectrum plays a more crucial role because the pump and signal pulses are both chirped, with PM inextricably occurring only between suitable spectral portions of the pump and the signal pulses that also overlap in the temporal domain.

With this in mind, the optimal selection of the Ti:sapphire pumping bandwidth and central wavelength in a BIBO-based OPCPA system involves two critical aspects:

1. Dispersion management. Gratings are not considered because of the relative high loss and the CEP variation that requires active stabilization [16]. Chirped mirrors are only good to compress a broadband pulse within a few bounces, because too many bounces will decrease pulse contrast significantly and also cause a high loss. Here the scheme of an acousto-optic programmable dispersive filter (AOPDF) as the stretcher plus a bulk material as a compressor is employed due to the adaptive phase control by AOPDF and high transmission and compactness of the bulk material. Unfortunately, many bulk materials have a zero-dispersion point near the short-wavelength side of the desired spectrum, such as SF-57 at 1.8  $\mu\text{m}$  and fused silica at 1.3  $\mu\text{m}$ , which results in large higher order dispersions. IR materials such as ZnSe do not have a zero-dispersion point over the desired spectrum, but they usually have very large nonlinear refractive index  $n_2$ , relatively low bandgap, and nonvanishing second-order nonlinearity  $\chi^{(2)}$ . As fused silica (small  $n_2$  and large bandgap) is chosen as the compressor, the OPCPA seed pulse must be nonlinearly stretched to match the inherent material dispersion, which complicates the PM in the temporal domain. Thus, the nonlinear chirp must be accounted for when choosing the bandwidth and central wavelength of the pump laser.

2. Design of pump bandwidth. While a narrow-band pump is more convenient for PM, stretching such a weakly polychromatic pulse to several hundred ps—necessary to avoid damaging the gain medium in the pump-producing chirped-pulse amplifier (CPA)—requires a large stretcher-compressor design. Thus, an appropriately broad pump bandwidth can facilitate the compactness of the CPA without sacrificing the PM efficiency.

To address the first design concern: the PM efficiency,  $\text{sinc}^2(\Delta kL/2)$ , is plotted as a function of the pump (bottom axis) and signal wavelengths (left axis) in Fig. 1(a), where  $\Delta k$  represents phase mismatch and  $L$  is the BIBO crystal length equal to 5 mm. The color contours represent the PM efficiency supported by a collinearly configured BIBO crystal with a phase-matching angle  $\theta = 10.9^\circ$ , and the black line demonstrates the group delay for a stretched signal pulse overlapped with a linearly stretched pump pulse for PM in the temporal domain (top axis). The most distinct feature of the stretched signal pulse is that the shorter wavelengths cannot be stretched as much as the longer wavelengths, due to the zero-dispersion point of the fused silica bulk compressor near 1.3  $\mu\text{m}$ . This sets a reference for determining the proper pump wavelengths for good PM in the temporal domain.

To address the second design concern: Fig. 1(a) also demonstrates that the pump bandwidth for achieving good PM is

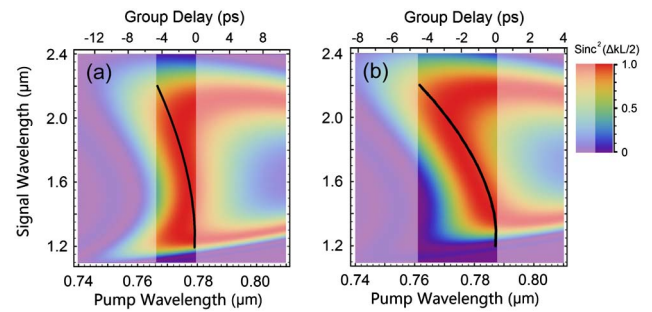


**Fig. 1.** The calculated PM efficiency as a function of pump and signal wavelengths for (a) the collinear configuration (PM angle  $\theta = 10.9^\circ$ , noncollinear angle  $\alpha = 0^\circ$ ); and (b) the noncollinear configuration (PM angle  $\theta = 10.82^\circ$ , noncollinear angle  $\alpha = 0.6^\circ$ ). The black line represents the chirped signal pulse with its corresponding wavelengths marked by the left axis and its temporal chirp marked by the top axis.

relatively narrow, as suggested by the unshaded area. To broaden the phase-matchable pump bandwidth, a noncollinear angle  $\alpha$  can be introduced to the BIBO in order to adjust the PM relationship between the pump and signal wavelengths. Figure 1(b) shows the noncollinear configuration with  $\alpha = 0.6^\circ$ , with the unshaded area indicating that the region of good PM (red contours) is stretched over a broader range of pump wavelengths compared to the collinear case in Fig. 1(a). Therefore, this optimized noncollinear configuration helps reduce the constraints on the pulse stretcher in the pump-producing CPA system.

To further study how the pump bandwidth influences the OPCPA gain and its bandwidth, a 1D three-wave mixing numerical model has been developed by modifying the previously developed one in [17]: (1) the model includes the effects of dispersion and nonlinear refractive index and excludes the effects of diffraction; (2) all three waves are assumed to be plane waves; and (3) the model only considers the OPCPA process discussed herein. The value of the effective second-order nonlinearity  $d_{\text{eff}}$  is equal to 2.11 pm/V. The signal pulse (1.2–2.2  $\mu\text{m}$ ) is stretched to 4.4 ps between 1.3  $\mu\text{m}$  and 2.2  $\mu\text{m}$ . The FWHM pump pulse is linearly chirped to 5 ps, under which the damage threshold is around 20 GW/cm<sup>2</sup> determined by the BIBO antireflection coating. The peak intensities of the signal and the pump are assumed to be 1.5 MW/cm<sup>2</sup> and 8 GW/cm<sup>2</sup>, respectively, in order to achieve a gain of around 1000 in a 5 mm BIBO first-stage amplifier. Figure 2(a) shows the simulated results using three pump spectra: (1) a 730–830 nm Gaussian pump spectrum typical of a home-built Ti:sapphire CPA described hereafter (green), (2) a 775–785 nm super-Gaussian spectrum for best PM (red), and (3) a 760–810 nm super-Gaussian spectrum that represents a compromise between the other two (blue). The power spectrum shapes of the pump laser are similar to the corresponding pump pulse shapes in the temporal domain shown in Fig. 2(b).

Compared to the ideal case of spectrum (2), the signal spectrum pumped by spectrum (1) is gain-narrowed and the gain is >25% smaller—both due to the poor PM at the wings of the spectrum and the nonflat pump pulse shape, which is indicated in Fig. 2(b). On the other hand, the amplified signal spectrum using spectrum (3) is similar to the one pumped by the ideal spectrum (2), with the gain only being <4% smaller—a matter easily compensated by using either a slightly higher pump

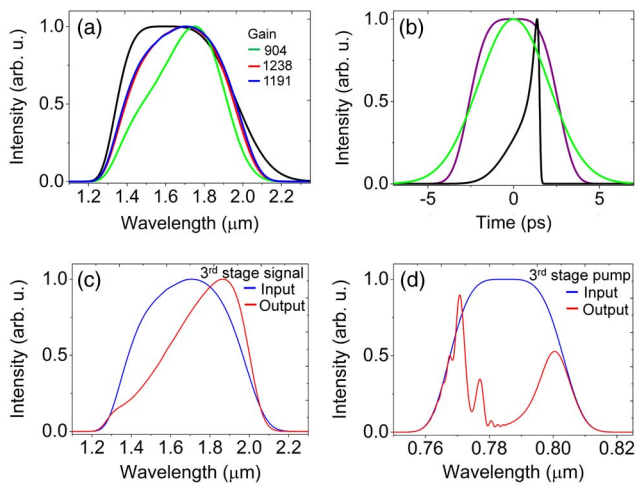


**Fig. 2.** Simulation of a first-stage OPCPA in a 5 mm BIBO: (a) input signal spectrum (black) and output signal spectrum when pumped by 775–785 nm (red), by 760–810 nm (blue), and by 730–830 nm (green); (b) temporal shape of the signal input pulse (black), the 775–785 nm and 760–810 nm pump pulse (purple), and the 730–830 nm pump pulse (green); (c) and (d) simulation of a third-stage OPCPA in a 3 mm BIBO.

intensity or a thicker crystal. Thus by using a bandpass filter to cut the 730–830 nm Gaussian spectrum to a 760–810 nm super-Gaussian spectrum, the home-built Ti:sapphire CPA can be outfitted for pumping a high-efficiency OPCPA without gain narrowing. Meanwhile, with a 360 ps (730–830 nm) stretcher-compressor design, a 180 ps pulse (760–810 nm) is safe enough to avoid damage in the high-energy CPA system.

To study the conversion efficiency that can be achieved in such an OPCPA pumped by a 760–810 nm super-Gaussian laser, we simulated the third-stage amplifier, as shown in Figs. 2(c) and 2(d). The peak intensities for the signal and pump are  $0.8 \text{ GW/cm}^2$  and  $7 \text{ GW/cm}^2$ , respectively. The BIBO thickness is 3 mm. With a high pump depletion, a conversion efficiency of 28% is achieved at the expense of a slightly gain-narrowed spectrum. The experimentally achievable conversion efficiency is expected to be lower, since it is determined by spatially integrated energy extraction from the pump to the signal and since other nonlinear processes, such as difference-frequency generation

(DFG), sum-frequency generation, and parasitic second-harmonic generation, are not included in the model.

To meet the requirements for such an OPCPA system, a three-stage Ti:sapphire CPA system is employed, as represented by the left side of Fig. 3. Nanojoule-level oscillator pulses (730–830 nm) are stretched to 360 ps in an Offner-type stretcher before the pulse energy is boosted to 4 mJ with a homemade 14-pass Ti:sapphire amplifier system. The central wavelength does not shift, because the Ti:sapphire crystal is cooled to 173 K by the cold finger of a liquid immersion chiller. The 4 mJ from the 14-pass amplifier is split into two beams. First, a 1.4 mJ portion is chopped to 760–810 nm with a flattop shape by a transmission filter; an energy of 21 mJ is achieved after two additional cryocooled amplifiers—a 6-pass and a 3-pass—before a transmission grating pair compresses the pulse to 5 ps (FWHM) with 18 mJ. This beam is split into three portions for pumping the three OPCPA amplifiers described in the next paragraph. Second, the remaining 2.6 mJ portion is compressed to 2.2 mJ, 30 fs by a transmission grating pair and then sent to a hollow-core fiber (HCF) filled with 30 psi neon for white light generation. The white light is compressed to  $\sim 7$  fs using chirped mirrors. A broadband IR (1.2–2.2  $\mu\text{m}$ ) seed with a pulse energy of around 1  $\mu\text{J}$  is generated via intrapulse DFG of the white light in a 1 mm type-II BIBO crystal (PM angle  $\theta = 60^\circ$ ). The seed is then stretched to 4.4 ps using an AOPDF with an output energy of  $\sim 50$  nJ.

The OPCPA is composed of three stages, each one consisting of a Type 1 BIBO crystal with a PM angle of  $\theta = 10.8^\circ$  and a small noncollinear angle of  $\alpha = 0.6^\circ$ . Both the first and second stages have 5 mm-thick BIBO crystals and are pumped by 360  $\mu\text{J}$  and 3.2 mJ, respectively. The output pulse energy of these stages are 30  $\mu\text{J}$  and 400  $\mu\text{J}$ , correspondingly. The second-stage output is further boosted from 400  $\mu\text{J}$  to 3 mJ in a 3 mm-thick BIBO pumped by 14.4 mJ pulse energy in the third OPCPA stage. The spectra at each stage are shown in Fig. 4. In this last stage, the highest energy (3 mJ) and conversion efficiency (18%) among any current near-octave OPCPA are achieved. The IR pulse is compressed in a 150 mm fused silica bulk compressor to a FWHM pulse duration of 11.4 fs as retrieved by a home-built second-harmonic-generation frequency-resolved optical gating (SHG FROG), whose trace is depicted in Fig. 5.

For CEP measurements, a single-shot f-to-2f interferometer is utilized in which a sapphire plate generates a white light

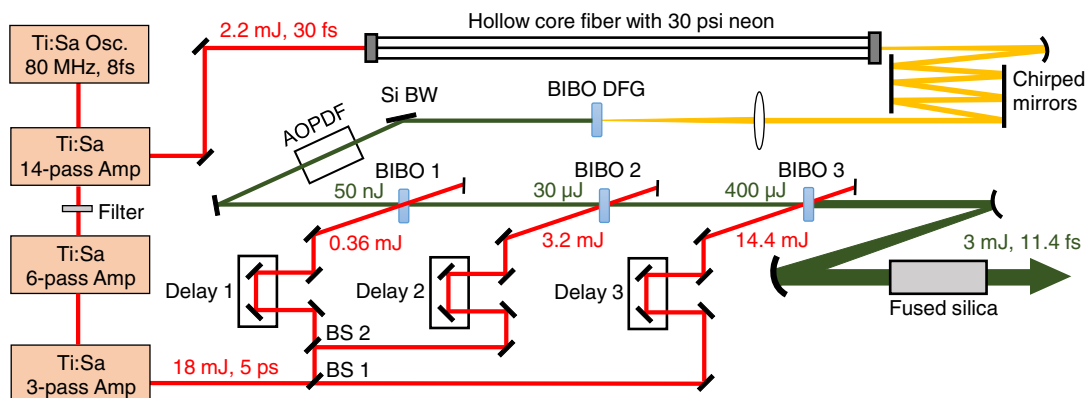


**Fig. 3.** Schematic setup of the OPCPA system. BS1, 20% reflection beam splitter; BS2, 10% reflection beam splitter; Si BW, silicon window at Brewster's angle.

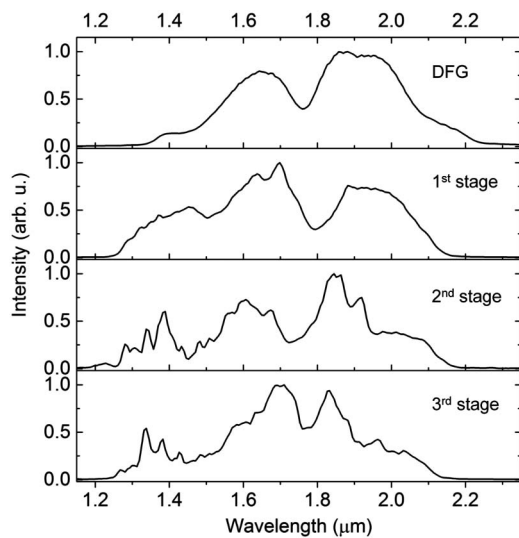


**Fig. 4.** Spectra taken at successive stages of the laser system.

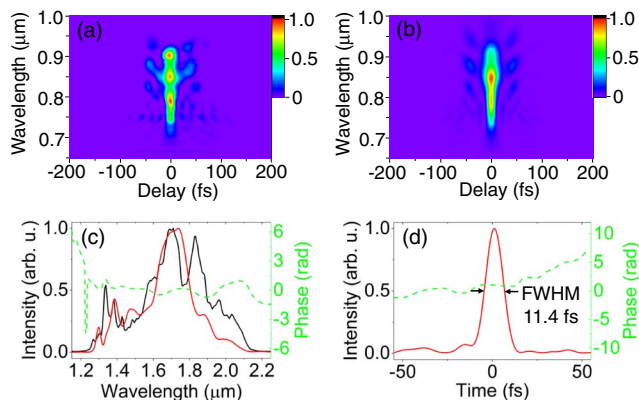


**Fig. 5.** (a) Experimental SHG FROG trace; (b) retrieved SHG FROG trace; (c) independently measured spectrum (black), retrieved spectrum (red), and retrieved spectral phase (green); (d) retrieved pulse (red) and temporal phase (green).

continuum, and a BBO crystal yields the frequency-doubled component. The CEP fluctuation is measured to be 165 mrad (RMS) after 1 h of single-shot collection, as shown in Fig. 6.

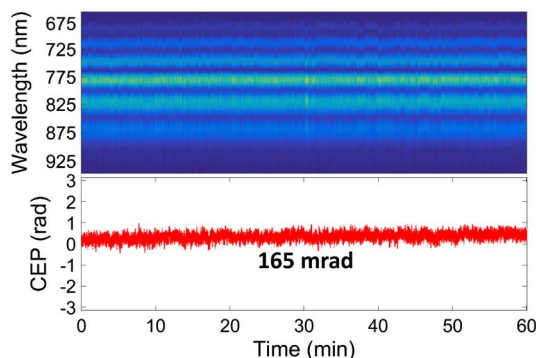


**Fig. 6.** Top: f-to-2f interferograms collected for 1 h; bottom: CEP fluctuations (165 mrad RMS) in 1 h.

To conclude, a high-efficiency, 3 mJ, two-cycle, 1 kHz, and CEP-stable IR OPCPA light source was developed with a central wavelength at 1.7  $\mu\text{m}$ . Scaling of the performance of this light source to over 10 mJ pulse energy is expected in the near future by enhancing the Ti:sapphire output energy to 60 mJ. Such a laser system paves the way for the generation of a bright broadband soft x-ray continuum covering the water-window region (280–530 eV), thus enabling attosecond pulses shorter than the atomic unit of time (24 as). This attosecond source itself poses a groundbreaking opportunity for ultratime-resolved spectroscopy of biologically relevant samples and strongly correlated solid-state materials.

**Funding.** Division of Physics (PHY) (1068604); Army Research Office (ARO) (W911NF-14-1-0383); Air Force Office of Scientific Research (AFOSR) (FA9550-15-1-0037); Defense Advanced Research Projects Agency (DARPA) (W31P4Q1310017).

**Acknowledgment.** The authors thank Prof. Jiro Itatani, Prof. Nobuhisa Ishii, and Dr. Yunpei Deng for sharing their experience in few-cycle OPCPA.

<sup>†</sup>These authors contributed equally to this work.

## REFERENCES

- Z. Chang and P. Corkum, *J. Opt. Soc. Am. B* **27**, B9 (2010).
- K. Zhao, Q. Zhang, M. Chini, Y. Wu, X. Wang, and Z. Chang, *Opt. Lett.* **37**, 3891 (2012).
- F. Silva, S. M. Teichmann, S. L. Cousin, M. Hemmer, and J. Biegert, *Nat. Commun.* **6**, 6611 (2015).
- B. Shan and Z. Chang, *Phys. Rev. A: At., Mol., Opt. Phys.* **65**, 011804 (2001).
- J. Tate, T. Augustine, H. G. Muller, P. Salières, P. Agostini, and L. F. DiMauro, *Phys. Rev. Lett.* **98**, 013901 (2007).
- A. D. Shiner, C. Trallero-Herrero, N. Kajumba, H.-C. Bandulet, D. Comtois, F. Légaré, M. Giguère, J.-C. Kieffer, P. B. Corkum, and D. M. Villeneuve, *Phys. Rev. Lett.* **103**, 073902 (2009).
- H. Fattahi, H. G. Barros, M. Gorjan, T. Nubbemeyer, B. Alsaif, C. Y. Teisset, M. Schultze, S. Prinz, M. Haefner, M. Ueffing, A. Alismail, L. Vámos, A. Schwarz, O. Pronin, J. Brons, X. T. Geng, G. Arisholm, M. Ciappina, V. S. Yakovlev, D.-E. Kim, A. M. Azzeer, N. Karpowicz, D. Sutter, Z. Major, T. Metzger, and F. Krausz, *Optica* **1**, 45 (2014).
- A. Vaupel, N. Bodnar, B. Webb, L. Shah, and M. Richardson, *Opt. Eng. (Bellingham, Washington, U.S.)* **53**, 051507 (2014).
- O. D. Mücke, S. Ališauskas, A. J. Verhoef, A. Pugžlys, A. Baltuška, V. Smilgevičius, J. Pocius, L. Giniūnas, R. Danielius, and N. Forget, *Opt. Lett.* **34**, 2498 (2009).
- Y. Deng, A. Schwarz, H. Fattahi, M. Ueffing, X. Gu, M. Ossiander, T. Metzger, V. Pervak, H. Ishizuki, T. Taira, T. Kobayashi, G. Marcus, F. Krausz, R. Kienberger, and N. Karpowicz, *Opt. Lett.* **37**, 4973 (2012).
- N. Ishii, K. Kaneshima, K. Kitano, T. Kanai, S. Watanabe, and J. Itatani, *Opt. Lett.* **37**, 4182 (2012).
- K.-H. Hong, C.-J. Lai, J. P. Siqueira, P. Krogen, J. Moses, C.-L. Chang, G. J. Stein, L. E. Zapata, and F. X. Kärtner, *Opt. Lett.* **39**, 3145 (2014).
- N. Ishii, K. Kaneshima, T. Kanai, S. Watanabe, and J. Itatani, *Conference on Lasers and Electro-Optics (CLEO: S&I)* (Optical Society of America, 2015), paper SF1M.3.
- A. Gaydardzhiev, I. Nikolov, I. Buchvarov, V. Petrov, and F. Noack, *Opt. Express* **16**, 2363 (2008).
- I. Nikolov, A. Gaydardzhiev, I. Buchvarov, P. Tzankov, F. Noack, and V. Petrov, *Opt. Lett.* **32**, 3342 (2007).
- C. Li, E. Moon, and Z. Chang, *Opt. Lett.* **31**, 3113 (2006).
- Y. C. Yin, D. French, and I. Jovanovic, *Opt. Express* **18**, 18471 (2010).